Role of Hydrophobic Partitioning in Substrate Selectivity and Turnover of the *Ricinus communis* Stearoyl Acyl Carrier Protein Δ^9 Desaturase†

Jeffrey A. Haas and Brian G. Fox*

The Institute for Enzyme Research, Graduate School, University of Wisconsin, Madison, Wisconsin 53705, and Department of Biochemistry, College of Agricultural and Life Sciences, University of Wisconsin, Madison, Wisconsin 53706

Received June 9, 1999; Revised Manuscript Received July 26, 1999

ABSTRACT: Stearoyl acyl carrier protein Δ^9 desaturase (Δ9D) uses a diiron center to catalyze the NADPH- and O_2-dependent desaturation of stearoyl acyl carrier protein (ACP) to form oleoyl-ACP. The reaction of recombinant *Ricinus communis* Δ9D with natural and nonnatural chain length acyl-ACPs was used to examine the coupling of the reconstituted enzyme complex, the specificity for position of double-bond insertion, the kinetic parameters for the desaturation reaction, and the selectivity for acyl chain length. The coupling of NADPH and O_2 consumption and olefin production was found to be maximal for 18:0-ACP, and the loss of coupling observed for the more slowly desaturated acyl-ACPs was attributed to autoxidation of the electron-transfer chain. Analysis of steady-state kinetic parameters for desaturation of acyl-ACPs having various acyl chain lengths revealed that the K_M values were similar (∼2.5-fold difference) for 15:0−18:0-ACP, while the k_{cat} values increased by ∼26-fold for the same range of acyl chain lengths. A linear increase in log (k_{cat}/K_M) was observed upon lengthening of the acyl chain from 15:0- to 18:0-ACP, while no further increase was observed for 19:0-ACP. The similarity of the k_{cat}/K_M values for 18:0- and 19:0-ACPs and the retained preference for double-bond insertion at the Δ^9 position with 19:0-ACP (>98% desaturation at the Δ^9 position) suggest that the active-site channel past the diiron center can accommodate at least one more methylene group than is found in the natural substrate. The $\Delta\Delta G_{binding}$ estimated from the change in k_{cat}/K_M for increasing substrate acyl-chain length was −3 kJ/mol per methylene group, similar to the value of −3.5 kJ/mol estimated for the hydrophobic partition of long-chain fatty acids (C-7 to C-21) from water to heptane [Smith, R., and Tanford, C. (1973) *Proc. Natl. Acad. Sci. U.S.A. 70,* 289−293]. Since the K_M values are overall similar for all acyl-ACPs tested, the progressive increase in hydrophobic binding energy available from increased chain length is apparently utilized to enhance catalytic steps, which thus provides the underlying physical mechanism for acyl chain selectivity observed with Δ9D.

Acyl-ACP[1] desaturases catalyze the NADPH- and O_2-dependent introduction of cis double bonds into saturated fatty acyl chains covalently attached to ACP via a phosphopantetheine thioester bond (*1*). These homodimeric enzymes are uniquely found in photoauxotrophic *Euglena* and the plastid organelles of plants. The acyl-ACP desaturases are also part of a functionally and structurally diverse group of soluble diiron enzymes (*2*) that includes the R2 component of ribonucleotide diphosphate reductase (*3*−*5*) and numerous bacterial hydrocarbon monooxygenases (*2*, *6*). These soluble enzymes have a closely related protein fold that contains two copies of the iron binding motif $(D/E)X_{\sim 40}EX_2H$ separated by ∼100 amino acids (*4*, *7*). All catalyze O_2 activation as part of their respective reaction cycles, and related intermediates including μ-1,2-peroxo, ferric-ferryl mixed valence, and diferryl have been recently identified (*2*, *6*, *16*, *60*−*62*), implying many aspects of the catalytic mechanisms will also be similar.

Stearoyl-ACP Δ^9 desaturase (Δ9D) is the best characterized acyl-ACP desaturase. This enzyme ($M_r \approx 84\,000$) preferentially desaturates stearoyl-ACP (18:0-ACP, $M_r \approx 9000$), yielding oleoyl-ACP (18:1-ACP). Spectroscopic studies have shown that resting Δ9D contains 4 mol of iron in two oxo/hydroxo-bridged diferric centers (*7*, *8*), while an X-ray structure revealed that photoreduced Δ9D had lost the oxo bridge (*9*). In this structure, the diferrous centers have two carboxylate bridges and each iron site has a five-coordinate, roughly octahedral geometry. A long nonpolar channel that nearly traversed the entire subunit was identified to contain the crystallization additive octyl glucoside. Molecular modeling showed that the dimensions of this channel

† This work was supported by Grant GM-50853 from the National Institutes of Health. B. G. F. is a Shaw Scientist of the Milwaukee Foundation (1994−1999). J.A.H. is a trainee of the NIH Institutional Molecular Biophysics Pre-Doctoral Training Grant T32 GM-08293.

* To whom correspondence should be addressed: E-mail fox@enzyme.wisc.edu; telephone (608) 262-9708; fax: (608) 265-2904.

[1] Abbreviations: ACP, holo-acyl carrier protein; ACP-His_6, recombinant acyl carrier protein containing a C-terminal His_6 sequence; *n*:0-ACP, an *n*-carbon saturated fatty acid covalently attached to acyl carrier protein through phosphopantetheine thioester bond; *n*:1-ACP, an *n*-carbon monounsaturated fatty acid covalently attached to acyl carrier protein; Δ9D, 18:0-acyl carrier protein Δ^9 desaturase; resting Δ9D, as-isolated form of 18:0-acyl carrier protein Δ^9 desaturase containing two diferric clusters; $4e^-$ Δ9D, chemically reduced form of 18:0-acyl carrier protein Δ^9 desaturase containing two diferrous clusters; EIMS, electron ionization mass spectrometry; Fd, recombinant *Anabaena* 7120 vegetative [2Fe-2S] ferredoxin; FdR, recombinant *Zea mays* NADPH:ferredoxin oxidoreductase.

10.1021/bi991318a CCC: $18.00
Published on Web 09/03/1999

were sufficient to accommodate an 18:0 acyl chain and place the C-9 position in proximity to the diiron center. Furthermore, mutagenesis has been used to alter the selectivity for chain length while retaining overall specificity for the position of double-bond insertion (*10*, *11*); the most productive of these mutations occur ~15 Å from the diiron center at the end of the nonpolar channel.

Recent MCD studies of $4e^-$ Δ9D produced by chemical reduction in the absence of 18:0-ACP revealed two equivalent, five-coordinate high-spin ferrous sites in a distorted square pyramidal geometry (*12*), which is consistent with the X-ray structure. Single-turnover catalytic studies have shown that $4e^-$ Δ9D is not reactive with O_2 in the absence of 18:0-ACP (*13*), implying that this equivalently coordinated diferrous state is not correctly configured for reactivity. Upon complexation with 18:0-ACP, changes in the MCD spectrum indicated the conversion of one iron site of the diferrous center from a five-coordinate site to a four-coordinate distorted tetrahedral geometry, while the other iron site was distorted toward a trigonal bipyramidal geometry; reaction of this complex with O_2 gives rise to a quasistable peroxo intermediate we have called peroxoΔ9D (*13*). Although the optical spectrum and the vibrational frequencies determined by resonance Raman spectroscopy are closely related to the μ-1,2 peroxo intermediates detected in other diiron enzymes (*14*−*17*), peroxoΔ9D decays by an oxidase reaction rather than by acyl chain desaturation. These spectroscopic studies indicate the possible physical consequences of 18:0-ACP binding on the structural properties of the diiron centers in $4e^-$ Δ9D and imply that substrate binding interactions may also provide substantial contributions to the catalytic desaturation cycle.

When compared to the presently available physical characterizations, considerably less information is available concerning the catalytic properties of Δ9D. In part, this has arisen from the complexity of obtaining sufficient quantities of acyl-ACPs. By combining previously defined enzymatic steps with newly available recombinant systems, we have been able to prepare both natural and nonnatural acyl-ACPs in large amounts (*18*). This availability has permitted the more extensive investigation of the steady-state kinetic properties of the Δ9D complex reported here.

During in vitro multiple turnover catalysis, a heterologous biological electron transfer chain consisting of FdR and [2Fe-2S] Fd has been established to provide minimally $2e^-$ to resting Δ9D (*19*, *20*). In this work, the conditions that yield either efficient coupling or rapid multiple turnover of the reconstituted, heterologous complex have been investigated. Furthermore, previous detailed kinetic studies of acyl-ACP desaturases have been limited to reactions of the safflower (*19*) and soybean isoforms (*20*) with the naturally occurring 16:0-ACP and 18:0-ACPs. These two independent studies suggested an ~100-fold increase in k_{cat} for 18:0-ACP as compared to 16:0-ACP, while the K_M values determined for these two substrates were similar. In light of this apparent kinetic selectivity for acyl chain length, and with respect to the newly available structural and spectroscopic data on Δ9D, we have undertaken a more detailed steady-state kinetic analysis of the Δ9D reaction. These studies, performed with acyl-ACPs having both natural and unnatural acyl chain lengths, reveal that hydrophobic binding energy is used to enhance catalysis rather than improve substrate binding. As the binding of shorter acyl chains apparently does not provide sufficient activation energy for efficient desaturase catalysis, these observations reveal the underlying mechanism for acyl chain length selectivity observed with Δ9D.

MATERIALS AND METHODS

Enzymes. Recombinant stearoyl-ACP Δ^9 desaturase and *Anabaena* 7120 vegetative Fd were expressed, purified, and characterized as previously described (*13*, *21*, *22*). Recombinant *Zea mays* FdR (*23*) was purified by a combination of ion exchange and gel filtration chromatographies. Recombinant *Leuconostoc mesenteroides* glucose-6-phosphate dehydrogenase was from Sigma Chemical Co. (St. Louis, MO).

Expression, Purification, and Acylation of ACP. For expression of *Escherichia coli* ACP,[2] the host was grown in a Bioflow 3000 fermenter (New Brunswick, Piscataway, NJ) in Luria−Bertani medium as previously described (*18*). *E. coli* ACP was produced as a mixture of the apo and holo forms and purified by minor modifications of established procedures (*24*; ~100 mg of purified ACP recovered/L of fermentation medium). Purification of spinach ACP·His_6, in vitro phosphopantetheinylation of either *E. coli* or spinach apo-ACP, and acylation of holo-ACPs with either 14:0−19:0 or 16:1 fatty acids were as previously described (*18*). Quantitation of acyl-ACP was performed by cleavage of the acyl chain in 0.06 M NaOH for 10 min at 40 °C followed by neutralization with HCl. The concentration of liberated free thiol on the phosphopantetheine group of holo-ACP was then quantitated by reaction with 5,5′-dithiobis(2-nitrobenzoic acid) (*25*).

Coupling Determinations. The coupling between NADPH and O_2 utilization and *n*:1-ACP production was determined at room temperature with a Clarke-type O_2 electrode (Yellow Springs Instruments, Yellow Springs, OH) and custom-built amplifier (*26*). The polarograph sensitivity was calibrated to provide full-scale response when 50 nmol of O_2 was consumed in the irreversible oxygenation of 50 nmol of recrystallized protocatechuic acid by purified 3,4 protocatechuate dioxygenase (*26*). A typical assay contained 4.4 nmol of FdR, 4.8 nmol of Fd, 4.5 nmol of Δ9D holoprotein, and 25 nmol of acyl-ACP in a final volume of 1.7 mL of 50 mM HEPES, pH 7.8, containing 50 mM NaCl. The reaction was initiated by the addition of 25 nmol of NADPH. After the O_2 consumption reaction was complete, the reaction mixture was removed from the electrode chamber and quenched by the addition of tetrahydrofuran, and the acyl chains were extracted, derivatized, and quantitiated as described below.

Assays Used for Kinetic Studies. In a typical assay, 0.2 nmol of FdR, 1 nmol of Fd, 0.02 nmol of Δ9D, 1−50 nmol of *n*:0-ACP, and 1700 nmol of NADPH were placed in an open 5 mL autosampler vial containing 1 mL of 50 mM HEPES, pH 7.8, and 50 mM NaCl. For substrates with low k_{cat} (14:0-, 15:0-, and 16:0-ACP), the protein components were increased to provide greater product formation with time. In addition, an NADPH regeneration system (*27*) consisting of 200−400 μM glucose 6-phosphate, 9 units of glucose-6-phosphate dehydrogenase, and 200−400 μM

[2] J. A. Haas, M. A. Frederick, and B. G. Fox, unpublished results.

NADPH was used to maintain a constant NADPH level during the reaction. Reaction vials were shaken at 100 rpm in a 25 °C water bath. The reactions were started by the addition of Δ9D and at timed intervals 200 μL aliquots were withdrawn and quenched by rapid mixing with 150 μL of tetrahydrofuran.

Analysis of Kinetic Data. Initial desaturation velocities were determined by linear least-squares fitting of the increase in *n*:1 product versus time over a 3 min period. Four time points were used for least-squares fitting. The steady-state kinetic parameters k_{cat} and K_M were determined by nonlinear least-squares fitting of the initial desaturation velocity and the substrate concentration data to the Michaelis−Menten equation, $v = k_{cat}[S]/(K_M + [S])$. In this work, the turnover number, k_{cat}, is expressed relative to diiron center concentration. Linear and nonlinear least-squares fitting were done with KaleidaGraph (Abelbeck Software, Reading, PA).

Acyl Chain Extraction, Derivatization, and Quantitation. Quenched assay samples were further diluted with 300 μL of deionized H_2O and the fatty acyl chains were reductively cleaved from ACP by addition of ∼5 mg of $NaBH_4$ (*28*). After incubation at 37 °C for 15 min, the remaining $NaBH_4$ was quenched by addition of 100 μL of 1 N HCl containing saturating NaCl and the sample was then converted to alkaline pH by the addition of 30 μL of 10 N NaOH. The fatty alcohols were recovered by two equal-volume extractions with $CHCl_3$. The pooled $CHCl_3$ aliquots were evaporated to dryness under N_2 at 40 °C and resuspended in 60 μL of hexane. The fatty alcohols were converted to silyl ether derivatives for gas chromatographic analysis by the addition of 2.5 μL of *N*-methyl-*N*-trimethylsilyltrifluoroacetamide. Excess acetamide reagent was quenched by the addition of 1 μL of methanol.

The silyl ether products were identified and quantitated on a Hewlett-Packard 6890 gas chromatograph equipped with a 7683 auto injector and a HP-5MS column (30 m × 0.25 mm, 0.25 μm film thickness) connected to either a flame ionization detector or a Hewlett-Packard 5973 electron ionization mass-sensitive detector. Either split or splitless injection was used depending on the quantity of silyl ether to be analyzed. For either injection method, the injector was maintained at 250 °C, the flame ionization detector was maintained at 300 °C, and the mass detector auxiliary temperature was maintained at 280 °C. The column temperature was held at 50 °C for 2 min following injection, increased to 200 °C at 35 °C/min, and then increased from 200 °C to 218 °C at 3 °C/min. Under these conditions, the 18:1- and 18:0-silyl ethers eluted at 15.9 and 16.5 min, respectively. The fractional desaturation of a fatty acid was calculated by dividing the *n*:1 peak area by the sum of *n*:0 plus the *n*:1 peak areas, and the total nanomoles of *n*:1-ACP formed during the reaction was calculated by multiplying the total nanomoles of *n*:0-ACP introduced into the reaction by the fractional conversion.

Determination of Double-Bond Position. To provide greater sensitivity to the accumulation of minor products in the positional analysis, enzyme reactions were scaled up ∼10-fold relative to the reaction mixture used for kinetic studies. Double-bond positions were determined by tandem GC-EIMS analysis of the bis(methylthio)derivatives of the products of 14:0-, 15:0-, 17:0-, and 19:0-ACP desaturation reactions (*29*). Fatty alcohols obtained from $NaBH_4$ treatment were resuspended in 100 μL of diethyl ether containing 60 mg/mL I_2 and then followed by the addition of 350 μL of dimethyl disulfide. The samples were shaken for 1 h at 37 °C and then the bis(methylthio) derivatives of the fatty alcohols were extracted, silylated, and analyzed by the methods and GC-EIMS instrument described above. The EIMS data were collected in scan mode with an ionization energy of 70 eV. During chromatographic separation, the column temperature was increased from 160 to 220 °C at 2 °C/min and then increased from 220 to 245 °C at 1 °C/min. Under these conditions, the bis(methylthio) derivatives of 15:1, 17:1, and 19:1 eluted at 30.8, 38.8, and 48.5 min, respectively. During the analysis of the 14:1 bis(methylthio) derivative, the column temperature was increased from 160 to 190 °C at 2 °C/min and then increased from 190 to 220 °C at 1 °C/min. Under these conditions, the 14:1 bis(methylthio) derivative eluted at 30.3 min.

Table 1: Coupling between O_2 Consumption and Acyl-ACP Desaturation[a]

acyl chain	O_2 consumed[b] (nmol)	desaturated product[c] (nmol)	coupling[d] (%)	rate[e] (nmol of O_2/min)
16:0	25.0 (1.9)	6.50 (2.0)	26	10.7 (1.3)
18:0	21.4 (0.11)	18.1 (1.1)	85	57.0 (9.9)
19:0	20.9 (0.19)	17.9 (0.049)	86	45.6 (0.85)

[a] Values reported are the average of duplicate experiments with the standard deviation in parentheses. [b] Amount of O_2 consumed in the presence of 25 nmol of acyl-ACP, 25 nmol of NADPH, and ∼4.5 nmol of FdR, Fd, and Δ9D. [c] Nanomoles of *n*:1 acyl chain produced. [d] Percentage of desaturated product relative to O_2 consumed. [e] The rate for O_2 consumption includes both coupled and uncoupled reactions. The reported values are ∼20% of k_{cat} determined for acyl chain desaturation by GC/EIMS under conditions where the electron-transfer chain and acyl-ACP were saturating.

RESULTS AND DISCUSSION

Performance of the Reconstituted Δ9D Complex. Recombinant proteins required to reconstitute the Δ9D complex are presently not available from a single organism. Thus the reconstituted complex typically consists of Δ9D and FdR from *Ricinus communis* and *Zea mays*, respectively, vegetative Fd from *Anabaena*, and acyl-ACP from either *E. coli* or spinach. Previous studies of the related diiron enzyme methane monooxygenase have shown that catalytic activity is exquisitely sensitive to protein component concentrations (*30*−*34*). It is therefore appropriate to consider the coupling efficiency of the heterologous Δ9D complex, particularly as uncoupled electron-transfer reactions may result in depletion of either NADPH or O_2 from the reaction mixtures or the accumulation of deleterious species such as H_2O_2 or O_2^-. Furthermore, in addition to positional specificity, binding affinity, and catalytic rate, coupling efficiency is a fundamental characterization that can provide significant insight into the mechanism of enzyme action (*35*−*38*) and the comparative function of mutated isoforms (*39*).

Table 1 shows the coupling of O_2 consumption and product formation determined for Δ9D with 16:0-, 18:0-, or 19:0-ACP as the substrate. For 18:0-ACP, 85% coupling between O_2 utilization and formation of the 18:1 desaturated product was obtained when the electron-transfer chain was configured to contain FdR, Fd, and Δ9D holoprotein in an equimolar ratio at micromolar concentrations. Under these conditions,

the coupling percentage for 19:0-ACP was nearly identical to that for 18:0-ACP (Table 1). For comparison, the camphor (*35*), methane (*36*), and toluene[3] monooxygenases also give high levels of coupling (~95%) at micromolar to submicromolar concentrations of the electron transfer, coupling, and monooxygenase components during oxidation of their preferred substrates. Since these bacterial enzymes are encoded by contiguous gene clusters that have likely been optimized by evolution for efficient catalytic function, the present Δ9D complex assembled from heterologous protein components performed reasonably well with 18:0-ACP as the substrate. However, when 16:0-ACP was used as the substrate with an otherwise identical electron-transfer chain composition, the coupling efficiency dropped to 26%.

The results of Table 1 demonstrate that the heterologous Δ9D complex investigated here can function as an efficiently coupled system only under defined experimental conditions, which in this case includes the appropriate choice of substrate, 18:0-ACP, and saturation of the electron-transfer chain with Δ9D. For 18:0- and 19:0-ACP, the rate of O_2 utilization during the well-coupled experiments was ~20% of the rate of 18:1 and 19:1 formation determined upon saturation of Δ9D with the electron-transfer chain. In the case of slow substrates such as 16:0-ACP or in the presence of excess amounts of the electron-transfer components, competing, uncoupled O_2 utilization reactions become significant relative to O_2 utilization coupled to desaturation. The loss of coupling efficiency is also observed during the oxidation of alternative substrates by P450 (*40*, *41*), flavoproteins (*42*), and other enzymes [e.g., 2-oxoglutarate-dependent enzymes (*2*)] that activate O_2 by reductive cleavage mechanisms. Furthermore, since steric packing has been proposed to contribute to the tight coupling observed in P450cam (*41*), the chain length dependence of coupling in Δ9D (Table 1) similarly suggests that efficient packing of the acyl chain in the active site may play a role in coupled Δ9D turnover independent of the function of the electron-transfer chain.

Position of Double-Bond Insertion. The double-bond positions in the products of 14:0-, 15:0-, 17:0-, and 19:0-ACP desaturation were identified through tandem GC-EIMS analysis of the bis(methylthio) derivatives. Figure 1 shows that the mass spectra for each of these alcohol-TMS derivatives contains a strong signal from the characteristic molecular ion. Furthermore, each derivative yielded a high-abundance $m/z = 261$ ion diagnostic for fragmentation at the Δ^9 position and a second fragment ion with m/z corresponding to the remainder of the molecule. In all four cases, >98% of the products contained a double bond at the Δ^9 position based on the low abundance of ions expected for double-bond insertion at alternative positions (between C-8 and C-9 or between C-10 and C-11, indicated by arrows in Figure 1D) as compared to the abundance of the $m/z = 261$ ion for double-bond insertion between C-9 and C-10. Thus strict conservation of regiospecificity at the Δ^9 position was observed, and in particular for 19:0-ACP desaturation. In combination with the results reported elsewhere for 16:0- and 18:0-ACP desaturations (*1*, *19*, *20*), these results firmly support the conclusion that protein−protein interactions between ACP and the surface of Δ9D help to provide the "carboxyl-counting" aspect of Δ9D catalysis (*9*, *20*, *43*). However, the retention of double-bond position observed with 19:0-ACP reveals that the active-site channel past the diiron center can accommodate at least one more methyl group without substantial degradation of either coupling efficiency (Table 1) or double-bond positional specificity (Figure 1D). A contrasting result has been observed for the *Thunbergia alata* 16:0-ACP Δ^6 desaturase when assayed with 17:0-ACP (*10*). In this case, 85% of 17:1-ACP product contained a double bond at the Δ^6 position, while ~15% occurred at the Δ^7 position. Moreover, the active-site mutations L118F/P179I, at the end of the Δ9D active-site channel, caused a 5% accumulation of an 18:1 product with a double bond at the Δ^{10} position (*10*).

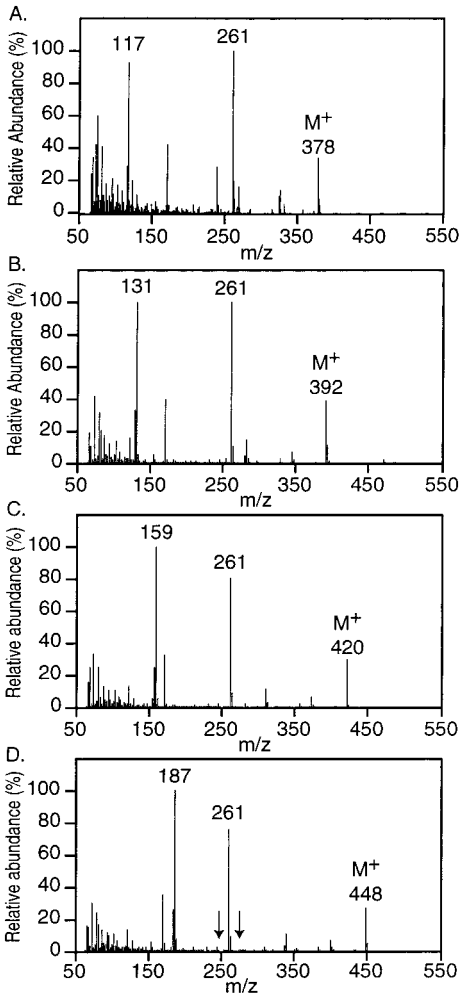

FIGURE 1: GC-EIMS spectra of trimethylsilyl, bis(methylthio) derivatives of acyl chains reductively cleaved from acyl-ACP following Δ9D-catalyzed desaturation. Products of Δ9D reaction with (A) 14:0-ACP, (B) 15:0-ACP, (C) 17:0-ACP, and (D) 19:0-ACP are shown.

Steady-State Kinetic Analysis. The GC-EIMS assay used for this study provides picomole sensitivity and chemical verification of products and thus offers an alternative to methods based on the use of radiolabeled fatty acids. To investigate whether electron-transfer reactions would be rate-limiting during steady-state kinetic measurements, $K_M = 0.38$ μM and $k_{cat} = 35$ min^{-1} were determined by varying Fd concentration in standard assays where the concentrations of all other protein components and substrates were fixed.

[3] J. M. Studts, J. D. Pikus, K. H. Mitchell, and B. G. Fox, unpublished results.

Subsequent analysis of the reactivity of 18:0-ACP under steady-state conditions showed that the k_{cat} for desaturation was nearly identical to the k_{cat} for electron transfer from Fd. Furthermore, the Fd concentration used in the kinetic assays was ~3-fold higher than the apparent K_M value, and increases in Fd concentration did not increase the rate of 18:0-ACP desaturation. Polarographic measurements revealed a chain-length-dependent fraction of total NADPH and O_2 utilization was being diverted to uncoupled turnover when the desaturation reaction was being driven at the maximal rate. Thus the reconstituted electron-transfer chain was not rate-limiting for desaturase catalysis.

For the faster substrates (17:0-, 18:0-, and 19:0-ACP), a constant rate of reaction and sufficient product formation were obtained in a 3 min assay for reliable kinetic analysis. No inhibitory effects were observed when a glucose-6-phosphate dehydrogenase-based NADPH regeneration system (*27*) was used to support 18:0-ACP desaturation. For the slower substrates (14:0-, 15:0-, and 16:0-ACP), the linearity of reaction could be maintained over longer time periods by use of higher concentrations of Δ9D, Fd, and FdR and the NADPH regeneration system, which also allowed accumulation of higher levels of products. This modification of the assay method was essential to obtain suitable kinetic behavior for the acyl-ACPs with acyl chains shorter than 17:0-ACP.

Figure 2A shows representative data for the time-dependent accumulation of 17:1 product during the desaturation of 17:0-ACP. The initial desaturation rate was determined by linear least-squares fitting of these data. Figure 2B shows a plot of the complete data set of initial desaturation rates versus 17:0-ACP concentrations; the nonlinear least-squares fit of these data to the Michaelis−Menten equation clearly demonstrates saturation behavior with respect to 17:0-ACP.

Table 2 shows the steady-state kinetic parameters k_{cat} and K_M determined for desaturation of 15:0- through 19:0-ACP; similar saturation behavior and quality of least-squares fits were observed for each of these acyl-ACPs. Comparison of the K_M values for 15:0- to 18:0-ACP revealed an ~2.5-fold variation between the maximum and minimum values as the length of the substrate acyl chain was changed. However, steady increases in k_{cat} and k_{cat}/K_M were observed as the substrate acyl-chain length was increased from 15:0 to 18:0, corresponding to an ~26-fold increase in both of these parameters. For 19:0-ACP, the calculated k_{cat}/K_M value was similar to that for 18:0-ACP, but this similarity arose from ~3-fold tighter binding in the Michaelis complex and a compensatory ~3-fold decrease in the maximal rate. Table 2 also shows kinetic parameters for the desaturation of spinach 18:0-ACP·His_6. The K_M value for this unnatural acyl-ACP isoform was similar to that determined for *E. coli* 18:0-ACP, while an ~25% increase in k_{cat} was observed for the spinach ACP·His_6 isoform.[4]

For the recombinant Δ9D isoform from castor, the ratio of k_{cat}/K_M values determined here for 18:0-ACP compared to 16:0-ACP is ~15. This selectivity is somewhat smaller than the 100-fold selectivity previously reported for the safflower (*19*) and soybean (*20*) isoforms purified directly from plant sources. While species-specific protein−protein interactions may contribute to these differences,[4] further comparisons of these results are appropriate. For the safflower isoform, the k_{cat}/K_M for *E. coli* 18:0-ACP (9.5 $\mu M^{-1}\cdot min^{-1}$) was in close agreement with that reported here

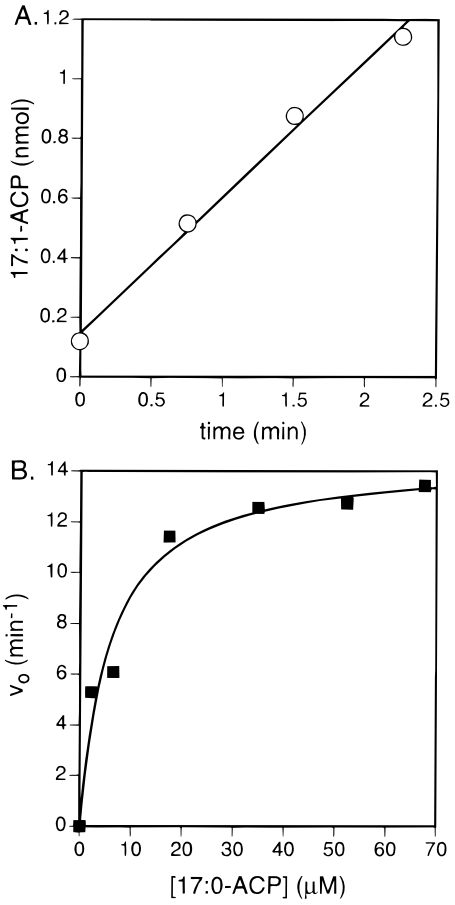

FIGURE 2: (A) Time-dependent accumulation of 17:1 desaturation product at a fixed initial 17:0-ACP concentration of 52 μM. (○) Nanomoles of 17:1 produced. The solid line is a linear least-squares fit whose slope is the initial desaturation rate, v_o. (B) dependence of v_0 on the concentration of 17:0-ACP substrate in Δ9D reaction. (■) Measured v_0 (min^{-1}). The solid line is a nonlinear least-squares fit to the Michaelis−Menten equation.

Table 2: Kinetic Parameters for Desaturation of Different Acyl-ACP Substrates by Stearoyl-ACP Δ^9 Desaturase[a]

substrate[b]	k_{cat}[c] (min^{-1})	K_M (μM)	k_{cat}/K_M ($\mu M^{-1}\cdot min^{-1}$)	R[d]
14:0[e]	0.43	5.8[f]	0.074[f]	—
15:0[e]	1.9 (0.010)	6.9 (0.16)	0.28	0.999
16:0[e]	5.7 (0.62)	8.3 (2.6)	0.69	0.983
17:0	14 (0.87)	5.9 (1.6)	2.5	0.984
18:0	33 (0.80)	3.3 (0.42)	10	0.988
18:0-sACP	49 (3.8)	3.9 (1.4)	13	0.969
19:0	12 (1.1)	1.3 (0.71)	9.4	0.931

[a] Errors reported in parentheses are derived from nonlinear least-squares fits as described in Materials and Methods. [b] All substrates were produced from recombinant *E. coli* ACP with the exception of 18:0-sACP, which was produced from recombinant spinach ACP·His_6. [c] k_{cat} per diiron active site. [d] Correlation coefficient from nonlinear least-squares fitting. [e] An NADPH regenerating system described in Materials and Methods was required to observe linear initial velocities due to the low k_{cat} value relative to uncoupled NADPH consumption. [f] Calculated as described in text.

[4] The small increase in k_{cat}/K_M observed for spinach 18:0-ACP versus *E. coli* 18:0-ACP is consistent with a minor contribution of protein−protein interactions, presently unspecified, to catalytic efficiency and selectivity. This role of protein−protein interactions has been recently elaborated for the production of unusual monoenoic fatty acids in certain plant tissues (*44*).

(Table 2, 10 $\mu M^{-1}\cdot min^{-1}$), but this similarity arose from a ~10-fold lower k_{cat} value and a 10-fold lower K_M value. For 16:0-ACP, the safflower isoform showed a 10-fold decrease in k_{cat} and essentially no change in K_M, which resulted in ~10-fold lower k_{cat}/K_M value (0.06 $\mu M^{-1}\cdot min^{-1}$) than that reported here (Table 2, 0.69 $\mu M^{-1}\cdot min^{-1}$). In these previous studies of the safflower isoform, the electron-transfer chain components, O_2, and NADPH were incubated for 10 min prior to the addition of acyl-ACP and Δ9D, which would allow for substantial uncoupled NADPH consumption, O_2 reduction, and potential inactivation reactions. As described above (Table 1), the uncoupled reactivity would be further exacerbated upon addition of 16:0-ACP, so that malfunction of the electron-transfer chain may account for the lower k_{cat} value. For the soybean isoform, the k_{cat} values determined for both 16:0- and 18:0-ACPs were comparable to those reported here, while the K_M values were ~4-fold higher. However, a 1.5-fold increase in the desaturation rate was noted when the Fd concentration was raised 5-fold in the presence of subsaturating concentrations of 18:0-ACP (*20*), suggesting that the magnitude of the K_M values may have been overestimated due to faulty optimization of the electron-transfer chain.

Inhibition of 18:0-ACP Desaturation by Holo-ACP, 14:0-ACP, or 16:1-ACP. The rate of desaturation of 40 μM 18:0-ACP was not changed by the addition of 40 μM holo-ACP to the assay and was reduced by only ~20% in the presence of 600 μM holo-ACP. This limited inhibition study supports the importance of the acyl chain to productive binding interactions between ACP and Δ9D. However, the rate of desaturation observed for 20 μM 18:0-ACP in either the presence or the absence of 20 μM 14:0-ACP was identical (data not shown), suggesting that the association and dissociation rates for 14:0-ACP are considerably faster than the subsequent catalytic steps (no 14:1 product was detected under the conditions optimized for 18:0 desaturation) and that 18:0-ACP may have considerably higher commitment to catalysis once the initial ES complex is formed (*45*). The inclusion of 16:1-ACP at four different fixed concentrations of 18:0-ACP resulted in an apparently mixed-type pattern of inhibition of the 18:0-ACP desaturation reaction. Further characterization of this inhibition mechanism was not undertaken for these studies.

Role of Hydrophobic Partitioning in Substrate Selectivity. Previous kinetic studies of the safflower and soybean isoforms of Δ9D have suggested a role for the substrate acyl chain in achieving optimal catalytic rates for desaturation, a V_{max} effect (*19*, *20*). Furthermore, a combination of mutagenic and crystallographic analyses of castor Δ9D have led to the proposal that interactions of the terminal methyl group of the substrate acyl chain with the end of the active-site channel control the chain length selectivity (*1*, *10*).

Figure 3 shows that there is a linear relationship between the length of the acyl chain of 15:0- through 18:0-ACP and the log (k_{cat}/K_M) values. The linearity of this plot for both natural and nonnatural acyl chain lengths supports the validity of the comparative steady-state kinetic analysis shown in Table 2 and Figure 2. The slope of this plot is equivalent to the hydrophobic substituent constant π, defined as $\pi = \log P_X - \log P_H$, where P_H is the partition coefficient of a parent molecule between an organic solvent and water and P_X is the partition coefficient of the derivative (*46*). Since π is

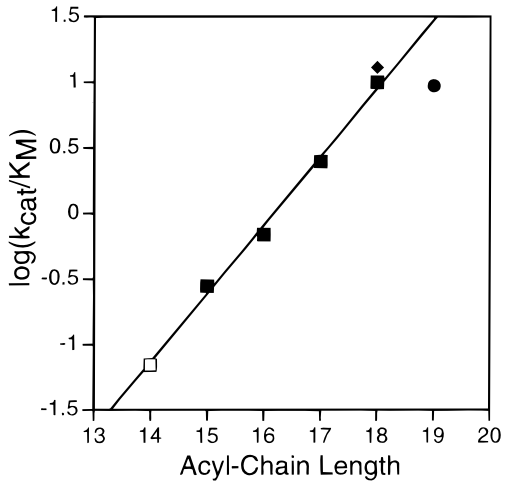

FIGURE 3: Dependence of log (k_{cat}/K_M) on the length of acyl-chain for natural and nonnatural acyl-ACP substrates. The solid line is a least-squares fit of the 15:0- to 18:0-ACP data showing a linear increase in log (k_{cat}/K_M) per methylene group added to the substrate. Symbols used are as follows: log (k_{cat}/K_M) values for 15:0- through 18:0-ACP (■); 18:0-sACP·His_6 (◆); 19:0-ACP (●). The log (k_{cat}/K_M) value for 14:0-ACP (□) was calculated as described in the text.

derived from equilibrium partition coefficients, it is also a thermodynamic constant. From partition coefficient analysis of a wide variety of parent compounds, a value of $\pi \approx 0.5$ per additional methylene group has been determined (*46*). π-constants have been used to measure the effect of changes in the hydrophobic substituents of substrates or inhibitors on enzyme catalysis (*46*, *47*). Recently, enzymes whose substrates have *n*-alkyl substituents of varying chain length have been analyzed by this approach (*48*−*50*). Like Δ9D, these enzymes also have a linear relationship between chain length and log (k_{cat}/K_M) over a defined range of *n*-alkyl chain lengths. The π-values determined for methylene group addition varied from 0.7 to 1.3 for the yeast and human isoforms of aldose reductase, respectively (*49*, *50*), while a π-value of ~1.5 was observed for nitroalkane oxidase (*48*). For each of these three enzymes, the observed increase in k_{cat}/K_M arose primarily from a decrease in K_M as the length of the alkyl chain was increased.

From the slope of the plotted line in Figure 3, a value of $\pi = 0.52$ was determined for Δ9D catalysis with 15:0−18:0-ACPs. In this case, the observed increase in k_{cat}/K_M arose primarily from an increase in k_{cat} as opposed to a decrease in K_M (Table 2). From the relationship $\Delta\Delta G_{binding} = -2.303RT\pi$ (*51*), a free energy change of ~−3 kJ/mol per methylene group may be available from binding interactions for enhancement of the Δ9D reaction. Similarly, a study of the hydrophobic partitioning of long-chain saturated fatty acids (C7−C21) between heptane and aqueous solutions revealed a monotonic increase in $\Delta\Delta G_{transfer}$ for increasing alkyl chain length corresponding to ~−3.5 kJ/mol per methylene group (*52*). Thus the π-value determined for the reaction of acyl-ACPs with Δ9D strongly implies a role for hydrophobic partitioning of the substrate acyl chain from aqueous solution into the nonpolar active-site channel (*9*). Since ^{19}F NMR studies of 6,6- and 13,13-difluorotetradecanoyl-ACPs have indicated that at least the first 13 carbons of the acyl chain interact with ACP (*53*), ~15 kJ/mol of hydrophobic binding energy would potentially be

available from partition of the solvent-exposed end of an 18:0 acyl chain into the Δ9D active-site channel. We propose that optimized utilization of this hydrophobic binding energy is responsible for the catalytic selectivity of Δ9D catalysis.[5]

The linear relationship shown in Figure 3 did not hold for 19:0-ACP, as a decrease in K_M (tighter binding) and a decrease in k_{cat} were the apparent consequences of an extra methylene group. Attempts to extend this analysis to include 20:0-ACP were unsuccessful as this substrate could not be prepared by enzymatic acylation methods. In contrast, 14:0-ACP could be readily prepared and was desaturated to yield 14:1-ACP with >98% positional specificity for Δ^9 double bond insertion (Figure 1A). Due to the presence of low-boiling contaminants derived from the derivatization reagent that interfered with quantitation of low 14:1 concentrations, k_{cat}/K_M could not be directly determined at low substrate concentrations (*54*), and likewise, an accurate determination of the K_M value for 14:0-ACP was not possible by using either nonlinear least-squares fitting or reciprocal plotting. However, by evaluation of the rate of desaturation for 50 μM 14:0-ACP, which should approximate saturation on the basis of the K_M values determined for other acyl-ACPs (Table 2), a k_{cat} value of 0.43 min^{-1} was determined for 14:0-ACP. By combining this k_{cat} value and the equation for the best-fit line to the chain length versus log (k_{cat}/K_M) data for 15:0- through 18:0-ACP, a K_M value of 5.8 ± 3 μM was then estimated for 14:0-ACP. The magnitude of this calculated K_M value falls within the range of the K_M values measured for other acyl-ACPs (3.3−8.3 μM, Table 2).

Evolutionary Consequences of Acyl Chain Selectivity. A number of variant acyl-ACP desaturases with selectivities for shorter chain acyl-ACPs and with specificities for double-bond insertion at different positions have recently been identified (*11*, *55*−*59*). These enzymes are undoubtedly evolved from an ancestral acyl-ACP desaturase gene, on the basis of the high amino acid sequence identity. Surprisingly, some of these isoforms may have considerably lower specific activities for their respective, preferred desaturation reactions than Δ9D has for 18:0-ACP desaturation (*11*, *57*, *59*). This may reflect a reduced metabolic requirement for these unusual fatty acids and a correspondingly low evolutionary pressure to maximize enzyme performance. Alternatively, the lower specific activities may reflect the short evolutionary time since the emergence of these higher plant isoforms, which has not permitted a full reoptimization of catalytic properties.

Recently, mutagenesis methods have provided significant insight into the molecular basis for the divergence of chain-length selectivity in the acyl-ACP desaturases (*10*, *11*, *59*). For Δ9D, the site-directed mutations L118F and P179I, two amino acids found at the end of the putative 18:0-ACP active site channel, gave a 15-fold increase in *specific activity* for 16:0-ACP but a corresponding ∼10-fold decrease in specific activity for 18:0-ACP (*10*). Furthermore, the specific activity of the altered L118F/P179I Δ9D with 16:0-ACP was still ∼3-fold lower than the specific activity of the native isoform with 18:0-ACP. It has also been shown that the mutation L118W caused a shift to nearly equivalent specific activities for desaturation of either 16:0- or 18:0-ACP but caused a ∼30-fold decrease in the specific activity for 18:0-ACP desaturation (*11*). In these mutagenesis studies, K_M values and coupling efficiencies were not evaluated. However, based on the selectivity analysis of Table 2 and Figure 3, one plausible reason for the lower activity of the mutated Δ9D isoforms (occluded active-site channel) and other natural acyl-ACP desaturase isoforms (selectivity for shorter acyl chains) may be that less binding energy is available for transition-state stabilization from partition of shorter portions of acyl chain.

Role of Acyl Chain Binding in the Mechanism of Acyl-ACP Desaturase Catalysis. We have recently described the formation and reactivity of a peroxo complex of Δ9D (*13*). The combination of $4e^-$ Δ9D, 18:0-ACP, and O_2 was required to produce this intermediate, and substitution of either holo-ACP or stearoyl-CoA did not elicit its appearance. Furthermore, the presence or absence of 18:0-ACP has also been shown to cause profound changes in the electronic and geometric properties of the Δ9D clusters (*12*, *13*, *62*). The steady-state kinetic studies reported here further elaborate the role of the acyl chain by correlating an increase in hydrophobic binding energy available from a longer acyl chain with an increase in the rate of desaturation. A correlation of the presently available spectroscopic and thermodynamic data suggests that one role of 18:0-ACP binding may be to help convert the diiron center into a configuration more reactive with O_2, possibly by promoting carboxylate shifts or other required ligand rearrangement reactions.

[5] In principle, the observed data could also be accounted for by a subtle nonproductive binding that failed to produce the "proper orientation" within the active-site ES complex without affecting the K_M-values. However, the regio- and stereoselectivity of the double-bond insertion reaction remained the same, even as the shorter chain lengths gave rise to lower k_{cat} values. This fidelity suggests that at least the first 10 carbons of the acyl moiety on the substrate are "properly" oriented with respect to the diiron oxidant. Thus it is likely that the changes in chain length discussed in this work must involve interactions at the end of the substrate channel up to ∼14 Å from the diiron active site.

ACKNOWLEDGMENT

We thank Professor W. W. Cleland for helpful discussions regarding measurement of initial velocities and the analysis of steady-state kinetic data.

REFERENCES

1. Shanklin, J., and Cahoon, E. B. (1998) *Annu. Rev. Plant Physiol. Plant Mol. Biol. 49*, 611−641.
2. Fox, B. G. (1997) in *Comprehensive Biological Catalysis* (Sinnott, M., Ed.) pp 261−348, Academic Press, London.
3. Bollinger, J. M., Jr., Edmondson, D. E., Huynh, B. H., Filley, J., Norton, J. R., and Stubbe, J. (1991) *Science 253*, 292−298.
4. Nordlund, P., and Eklund, H. (1995) *Curr. Opin. Struct. Biol. 5*, 758−766.
5. Andersson, M. E., Högbom, M., Rinaldo-Matthis, A., Andersson, K. K., Sjöberg, B.-M., and Nordlund, P. (1999) *J. Am. Chem. Soc. 121*, 2346−2352.
6. Wallar, B. J., and Lipscomb, J. D. (1996) *Chem. Rev. 96*, 2625−2657.
7. Fox, B. G., Shanklin, J., Ai, J., Loehr, T. M., and Sanders-Loehr, J. (1994) *Biochemistry 33*, 12776−12786.
8. Shu, L., Broadwater, J. A., Achim, C., Fox, B. G., Münck, E., and Que, L., Jr. (1998) *J. Biol. Inorg. Chem. 3*, 392−400.
9. Lindqvist, Y., Huang, W., Schneider, G., and Shanklin, J. (1996) *EMBO J. 15*, 4081−4092.
10. Cahoon, E. B., Lindqvist, Y., Schneider, G., and Shanklin, J. (1997) *Proc. Natl. Acad. Sci. U.S.A. 94*, 4872−4877.

11. Cahoon, E. B., Shah, S., Shanklin, J., and Browse, J. (1998) *Plant Physiol. 117*, 593−598.
12. Yang, Y.-S., Broadwater, J. A., Fox, B. G., and Solomon, E. I. (1999) *J. Am. Chem. Soc. 121*, 2770−2783.
13. Broadwater, J. A., Ai, J., Loehr, T. M., Sanders-Loehr, J., and Fox, B. G. (1998) *Biochemistry 37*, 14664−14671.
14. Moënne-Loccoz, P., Baldwin, J., Ley, B. A., Loehr, T., and Bollinger, J. M., Jr. (1998) *Biochemistry 37*, 14659−14663.
15. Möenne-Loccoz, P., Krebs, K., Herlihy, K., Edmondson, D. E., Theil, E. C., Huynh, B. H., and Loehr, T. M. (1999) *Biochemistry 38*, 5290−5295.
16. Valentine, A. M., Stahl, S. S., and Lippard, S. J. (1999) *J. Am. Chem. Soc. 121*, 3867−3887.
17. Lee, S.-K., and Lipscomb, J. D. (1999) *Biochemistry 38*, 4423−4432.
18. Broadwater, J. A., and Fox, B. G. (1998) *Protein Expression Purif. 15*, 314−326.
19. McKeon, T. A., and Stumpf, P. K. (1982) *J. Biol. Chem. 257*, 12141−12147.
20. Gibson, K. J. (1993) *Biochim. Biophys. Acta 1169*, 231−235.
21. Hoffman, B. J., Broadwater, J. A., Johnson, P., Harper, J., Fox, B. G., and Kenealy, W. R. (1995) *Protein Expression Purif. 6*, 646−654.
22. Cheng, H., Westler, W. M., Xia, B., Oh, B.-H., and Markley, J. L. (1995) *Arch. Biochem. Biophys. 316*, 619−634.
23. Ritchie, S. W., Redinbaugh, M. G., Shiraishi, N., Vrba, J. M., and Campbell, W. E. (1994) *Plant Mol. Biol. 26*, 679−690.
24. Hill, R. B., MacKenzie, K. R., Flanagan, J. M., Cronan, J. E., Jr., and Prestegard, J. H. (1995) *Protein Expression Purif. 6*, 394−400.
25. Ellman, G. L. (1959) *Arch. Biochem. Biophys. 82*, 70−77.
26. Whittaker, J. W., Orville, A. M., and Lipscomb, J. D. (1990) *Methods Enzymol. 188*, 82−88.
27. Wong, C., and Whitesides, G. M. (1981) *J. Am. Chem. Soc. 103*, 4890−4899.
28. Barron, E. J., and Mooney, L. A. (1968) *Anal. Chem. 40*, 1742−1744.
29. Francis, G. W. (1981) *Chem. Phys. Lipids 29*, 369−374.
30. Fox, B. G., Froland, W. A., Jollie, D. R., and Lipscomb, J. D. (1990) *Methods Enzymol. 188*, 191−202.
31. Froland, W. A., Andersson, K. K., Lee, S.-K., Liu, Y., and Lipscomb, J. D. (1992) *J. Biol. Chem. 267*, 17588−17597.
32. Liu, Y., Nesheim, J. C., Lee, S.-K., and Lipscomb, J. D. (1995) *J. Biol. Chem. 270*, 24662−24665.
33. Liu, Y., Nesheim, J. C., Paulsen, K. E., Stankovich, M. T., and Lipscomb, J. D. (1997) *Biochemistry 36*, 5223−5233.
34. Davydov, R., Valentine, A. M., Komar-Panicucci, S., Hoffman, B. M., and Lippard, S. J. (1999) *Biochemistry 38*, 4188−4197.
35. Atkins, W. M., and Sligar, S. G. (1987) *J. Am. Chem. Soc. 109*, 3754−3760.
36. Fox, B. G., Froland, W. A., Dege, J. E., and Lipscomb, J. D. (1989) *J. Biol. Chem. 264*, 10023−10033.
37. Green, J., and Dalton, H. (1985) *J. Biol. Chem. 260*, 15795−15801.
38. Elgren, T. E., Lynch, J. B., Juarez-Garcia, C., Münck, E., Sjöberg, B.-M., and Que, L., Jr. (1991) *J. Biol. Chem. 266*, 19265−19268.
39. Sono, M., Roach, M. P., Coulter, E., and Dawson, J. H. (1996) *Chem. Rev. 96*, 2841−2887.
40. Fruetel, J. A., Collins, J. R., Camper, D. L., Loew, G. H., and Ortiz de Montellano, P. R. (1992) *J. Am. Chem. Soc. 114*, 6987−6993.
41. Loida, P. J., and Sligar, S. G. (1993) *Biochemistry 32*, 11530−11538.
42. Kamin, H., White-Stevens, R. H., and Presswood, R. P. (1978) *Methods Enzymol. 53*, 527−543.
43. Cahoon, E. B., and Ohlrogge, J. B. (1994) *Plant Physiol. 104*, 827−837.
44. Suh, M. C., Schultz, D. J., and Ohlrogge, J. B. (1999) *Plant J. 17*, 679−688.
45. Northrup, D. B. (1977) in *Isotope Effects on Enzyme-Catalyzed Reactions*, (Cleland, W. W., O'Leary, M., and Northrup, D. B., Eds.) pp 122−157, University Park Press, Baltimore, MD.
46. Hansch, C., and Fujita, T. (1964) *J. Am. Chem. Soc. 86*, 1616−1626.
47. Hansch, C., and Coats, E. (1970) *J. Pharm. Sci. 59*, 731−743.
48. Gadda, G., and Fitzpatrick, P. F. (1999) *Arch. Biochem. Biophys. 363*, 309−313.
49. Srivastava, S., Watowich, S. J., Petrash, J. M., Srivastava, S. K., and Bhatnagar, A. (1999) *Biochemistry 38*, 42−54.
50. Neuhauser, W., Haltrich, D., Kulbe, K. D., and Nidetzky, B. (1998) *Biochemistry 37*, 1116−1123.
51. Fersht, A. (1985) in *Enzyme Structure and Mechanism*, 2nd ed., p 475, W. H. Freeman, New York.
52. Smith, R., and Tanford, C. (1973) *Proc. Natl. Acad. Sci. U.S.A. 70*, 289−293.
53. Gally, H. U., Spencer, A. K., Armitage, I. M., Prestegard, J. H., and Cronan, J. E., Jr. (1978) *Biochemistry 17*, 5377−5382.
54. Cleland, W. W. (1975) *Biochemistry 14*, 3220−3224.
55. Cahoon, E. B., Shanklin, J., and Ohlrogge, J. B. (1992) *Proc. Natl. Acad. Sci. U.S.A. 89*, 11184−11188.
56. van de Loo, F. J., Fox, B. G., and Somerville, C. (1993) in *Lipid Metabolism in Plants*, (Moore, T. E., Ed.) pp 91−126, CRC Press, Boca Raton, FL.
57. Cahoon, E. B., Cranmer, A. M., Shanklin, J. B., and Ohlrogge, J. B. (1994) *J. Biol. Chem. 269*, 27519−27527.
58. Schultz, D. J., Cahoon, E. B., Shanklin, J., Craig, R., Cox-Foster, D. L., Mumma, R. O., and Medford, J. I. (1996) *Proc. Natl. Acad. Sci. U.S.A. 93*, 8771−8775.
59. Cahoon, E. B., Coughlan, S. J., and Shanklin, J. (1997) *Plant Mol. Biol. 33*, 1105−1110.
60. Que, L., Jr., and Dong, Y. (1996) *Acc. Chem. Res. 29*, 190−196.
61. Kurtz, D. M., Jr. (1997) *J. Biol. Inorg. Chem. 2*, 159−167.
62. Broadwater, J. A., Achim, C., Münck, E., and Fox, B. G. (1999) *Biochemistry* (in press).

BI991318A